Journal of Theoretical, Experimental, and Applied Physics ISSN: 3070-6505

PRIME OPEN ACCESS

Volume 2, Issue 1

Research Article

Date of Submission: 23 Jan, 2026
Date of Acceptance: 18 Feb, 2026
Date of Publication: 04 Mar, 2026

Second-Neighbor Hopping Effects on the Dynamics of Breathers in 2D Quantum Ultracold Atoms Loaded in Optical Lattices

Z I Djoufack[1,4*], J P Nguenang[2] and A Kenfack Jiotsa[3]

[1]African Institute for Mathematical Sciences, 6 Melrose, Muizenberg, South Africa

[2]Pure Physics Laboratory: Group of Nonlinear physics and Complex systems, Department of Physics, University of Douala, Cameroon

[3]Nonlinear physics and Complex systems, Department of Physics, The Higher Teachers' Training College, University of Yaounde I, Cameroon

[4]Unité de Recherche d'automatique et d'Informatique appliquée (UR-AIA), Fotso Victor University Institute of Technology P.O. Box 134 Bandjoun, University of Dschang, Cameroon

***Corresponding Author:** Z I Djoufack, African Institute for Mathematical Sciences, 6 Melrose, Muizenberg, South Africa.

Citation: Djoufack, Z. I., Nguenang, J. P., Jiotsa, K. A. (2026). Second-Neighbor Hopping Effects on the Dynamics of Breathers in 2D Quantum Ultracold Atoms Loaded in Optical Lattices. *J Theor Exp Appl Phys, 2*(1), 01-23.

Abstract

We explore analytically and numerically the dual role played by the second-neighbor hopping on the modulation instability and on the dynamics of breathers in 2D quantum ultracold atoms loaded in optical lattices. Via the linear stability analysis, it is shown that the dispersion relation formed exhibits intriguing forms. It is found that, the existence conditions of appearance of the modulational instability (MI) regions and the growth rate may be significantly affected by the second neighbor hopping coupling strength. To support the analytical studies, direct numerical simulations of MI is carried out to show the generation of a train of short waves exhibiting periodic W-shaped and V-shaped solitons with decreasing amplitude as time evolves. The emergence of breathers in the regions where the MI manifests is predicted to be influenced by the second neighbor hopping coupling strength. By making use of Rayleigh-Ritz variational method and in agreement with the MI analysis, the analytical results reveal the existence of the radial symmetric modes called the dynamics of breathers. The accuracy of the outcomes is checked by numerical calculations which show a good agreement with the theoretical analysis.

Keywords: Dynamics of Breathers, Modulational Instability, Optical Lattice, Quantum Ultracold Atoms

Introduction

Ever since the first experimental observation of Bose-Einstein condensation in the nineties, ultracold atomic gases in optical lattices have been the subject of intense research, issuing as only instrument to understand how the matter can be governed by the laws of quantum mechanics, thus representing a desirable platform to study of collective effects in many-body quantum physics systems as well as in the Mott-insulator and superfluid transition [1-8]. In this way, Bloch has shown that the production of a quantum lattice gas can be provided by an ultracold atom loaded into optical lattice [9,10]. An optical lattice can be formed by pairs of counter-propagating laser beams by creating an effective potential that traps ultracold atoms [11].

Generally, the dynamics of an ultracold bosonic atoms loaded in an optical lattice, are usually described by the Bose-Hubbard model or its extended models, for instance in the limit of a sufficiently deep optical lattice [4]. More recently, Prestipino revealed the existence of insulating phases with polyhedral order and a widely extended super solid region via the ground-state analysis in its work Bose-Hubbard model on polyhedral graphs [12].

However, ultracold atoms in optical lattices in the classical limit, can be approximated to a large number of bosons and usually explored by using the discrete nonlinear Schr¨odinger equation [13]. Discrete nonlinear Schr¨odinger equation in the classical nonlinear lattices admits discrete breathers' solution. These nonlinear discrete excitations, are time periodic and

spatially localized solutions of the classical nonlinear lattices [14,15]. Their existence in 1D nonlinear lattices was firstly established by Mackay and Aubry [16]. Discrete breather has been the subject of intense research on which several techniques have been developed to prove their existence. For instance, in quantum ultracold bosonic atoms in optical lattices, the quantum signature of breathers has been strongly reported in references [17–20].

In the physical point of view, it is shown that discrete breathers can be directly linked to the Modulation Instability (MI) of the plane's waves [21–24]. The MI can be defined by nonlinear excitations characterized by an exponential growth of amplitude perturbations caused by the interplay between the dispersion and nonlinearity during its propagation [25–27]. This phenomenon can be used as the best mechanism toward the formation of discrete breathers in many physical systems and has been discovered in deep water by Benjamen and his co-worker Feir in 1967 [28]. Their work has opened up fascinating windows in development of MI in deep water and in a large number of nonlinear systems [29,30]. From these latter researches, one can conclude that the MI seems to be best process to predict the formation of breathers in nonlinear system.

However, in 2D quantum ultracold atoms loaded in optical lattices usually describes by the Bose-Hubbard model, in any case, the number of studies devoted to solitons or breathers and MI in 2D lattice systems is comparatively smaller and very less investigated in 2D ultracold atoms and motivate us to explore more this area of research.

Only a few works in 2D Hubbard model are based on superconductivity in the way that, this model has played an important role in elucidating many aspects of superconductivity, on renormalization-group analysis, on topological states in optical lattices, on entanglement spectrum and phase diagram were studied in ultracold atoms [31-35]. More recently, by using the linear stability analysis, we have investigated on the MI and discrete breathers in 2D quantum ultracold atoms by taking only into account the effects of nearest neighbor interactions [36]. However, studies of MI and discrete breathers in 2D quantum ultracold atoms while extending the range of interaction over the first neighbor, and especially when considering the next-nearest neighbor (NNN) hopping is still missing.

In the Bose-Hubbard model, which is more adapted to describe quantitatively the role played by the lattice potential, the atomic repulsion and attraction, the kinetic energy in addition to the phase transition of particles in a lattice, the introduction of the NNN hopping may influence the properties of phase diagram, on the ground-state energy and on the quasi-particle [37]. It was shown by Kibey et al. that, the inclusion of the NNN interactions in β-Fermi-Pasta-Ulam quantized lattice reduces the Brillouin zone to half and changes the lattice periodicity and its effect on the eigenspectral [38]. The NNN hopping may also increase the superconducting gap. In 2D Hubbard model, Lin and his-coworker have shown that, the presence of NNN hopping in lattice has for role to rapidly decrease the magnitude of the hopping with distance [39]. Very recently, in the attractive 2D Hubbard Model, it is demonstrated that the NNN hopping gives rise to subtle effects, such as the breakdown of particle hole symmetry and the destruction of Fermi surface nesting at half filling [40]. In the extended Hubbard model, the importance of nearest and next-nearest-neighbor off-site interactions (diagonal and off-diagonal) has also been emphasized both from experimental results. In the magnetic spin chains, the introduction of the NNN interaction may affect the lattice periodicity, the properties of quantum soliton, and the energy spectrum [41,42]. Similar results were obtained in electrical nonlinear transmission line [43]. Some experiments and theories have suggested that by increasing the range of the interaction to include the second nearest neighbor in the graphene 2D honeycomb lattice may alternate the dispersion relation by removing dispersion symmetry around the Fermi level [44,45].

From the foregoing, this domain is still less investigated up to now and therefore attracts our interest to explore the MI and the dynamics of breathers in 2D quantum ultracold atoms loaded in optical lattices containing second neighbor hopping in order to improve knowledge in the field. We predict that, the inclusion of NNN hopping in a such optical lattices may affect some properties of MI as well as properties of the breathers dynamics.

The purpose of this paper is, to study the effects of second-neighbor hopping on the MI and on the dynamic's properties of breathers in 2D quantum ultracold atoms loaded in optical lattices.

The layout of the paper is organized as follows: In section 2, the Hamiltonian model of a 2D ultracold atoms loaded in an optical lattice with second neighbor hopping is defined and the equation of motion is obtained by using the Glauber's coherent state method. In section 3, by using linearized stability analysis, the existence condition for the appearance of MI of the system is found in addition to the effects of second-neighbor hopping on the MI of the system. Taking into account the fact that, the linear stability analysis cannot give more information of the long-time evolution of a modulated nonlinear wave, to examine the validity of a linear stability analysis, the direct numerical simulation of MI is carried out in section 4, whereas in section 5, by means of semi-discrete approximation combined to multiple-scale method, the 2D nonlinear schr¨0dinger equation (NLSE) including second-neighbor hopping is obtained and the existence conditions

of 2D discrete breathers are also discussed. The dynamics of breathers is examined by making use of Rayleigh Ritz variational method in addition to a numerical simulation to perform the analytical analysis in section 6. Section 7 presents the final conclusion and discussion.

Mathematical Model and Equation of Motion

The generalized model describing the dynamic of bosonic atoms on the optical lattices, can be modeled by the interacting bosons in a potential known as Bose-Hubbard model, where its quantized Hamiltonian of ultracold atoms loaded in 2D optical lattice with second-neighbor hopping is read

$$\widehat{H} = -t_x \sum_{(i,j)} \left(\widehat{a}^{\dagger}_{i,j}\widehat{a}_{i+1,j} + \widehat{a}_{i,j}\widehat{a}^{\dagger}_{i+1,j}\right) \quad (1)$$
$$-t_y \sum_{(i,j)} \left(\widehat{a}^{\dagger}_{i,j}\widehat{a}_{i,j+1} + \widehat{a}_{i,j}\widehat{a}^{\dagger}_{i,j+1}\right) - t_x^{'} \sum_{(i,j)} \left(\widehat{a}^{\dagger}_{i,j}\widehat{a}_{i+2,j} + \widehat{a}_{i,j}\widehat{a}^{\dagger}_{i+2,j}\right)$$
$$-t_y^{'} \sum_{(i,j)} \left(\widehat{a}^{\dagger}_{i,j}\widehat{a}_{i,j+2} + \widehat{a}_{i,j}\widehat{a}^{\dagger}_{i,j+2}\right) - \mu \sum_{r=(i,j)} \widehat{n}_r + \frac{U}{2} \sum_{r=(i,j)} \widehat{n}_r(\widehat{n}_r - 1),$$

where $\widehat{H}$, stands for the Hamiltonian, $\widehat{a}^{\dagger}_{i,j}$ and $\widehat{a}_{i,j}$ are the bosonic creation and annihilation operators, respectively verifying the following commutation relations $[\widehat{a}_{i,j}, \widehat{a}^{\dagger}_{i',j'}] = \delta_{ij}\delta_{i'j'}$, $[\widehat{a}^{\dagger}_{i,j}, \widehat{a}^{\dagger}_{i',j'}] = [\widehat{a}_{i,j}, \widehat{a}_{i',j'}] = 0$. U is the on-site interaction and represents the energy interaction of two bosons located in the same site (i, j). The system is repulsive for $U > 0$ and attractive for $U < 0$, $r = (i, j)$ stand for the lattice coordinates where as, t_x, t_y, $t_x^{'}$, $t_y^{'}$ the hopping amplitudes in the x and y direction. μ is the chemical potential.

$\widehat{n}_r = \widehat{a}^{\dagger}_{i,j}\widehat{a}_{i,j}$ represents the atomic number operator counting the number of atoms on the (i, j)th lattice site.

By adopting the Glauber's coherent state method for bosonic operators generally used to describe the components of quantum state [46]. In the case of ultracold atoms in 2D optical lattices, it can be defined as:

$$\widehat{a}_{i,j}|\Phi_{i,j}\rangle = \Phi_{i,j}|\Phi_{i,j}\rangle|\Phi_{i,j}\rangle,$$
$$\widehat{a}^{\dagger}_{i,j}|\Phi_{i,j}\rangle = \Phi^{*}_{i,j}|\Phi_{i,j}\rangle|\Phi_{i,j}\rangle, \quad (2)$$
$$|\Phi_{i,j}\rangle = \exp\Big(-\frac{1}{2}|\Phi_{i,j}|^2\Big) \sum_{l=1}^{\infty} \frac{(\Phi_{i,j})^l}{\sqrt{l!}}|l\rangle,$$

with, Φ_{ij} the coherent amplitude of the $\widehat{a}_{i,j}$ operator in the case where the system is in the state $|\Phi_{i,j}\rangle$. The quantum state $|\Psi(t)\rangle$ can be written as the following product of the multimode coherent state in the coherent state representation as:

$$|\Psi(t)\rangle = \prod_{i,j} |\Phi_{i,j}\rangle, \quad (3)$$

where $\langle\Psi(t)|\Psi(t)\rangle = 1$ should be normalized. With the aid of Ehrenfest's theorem [47], the dynamics of the system in terms of the Heisenberg equation of motion as function of the Bose operator annihilation $\widehat{a}_{i,j}$ can be written as follows:

$$i\frac{d\langle\widehat{a}_{i,j}\rangle}{dt} = \langle[\widehat{a}_{i,j}, \widehat{H}]\rangle \quad (4)$$
$$= F\big(\widehat{a}^{\dagger}_{i,j}, \widehat{a}_{i,j}, \widehat{a}^{\dagger}_{i+1,j}, \widehat{a}_{i+1,j}, \widehat{a}^{\dagger}_{i,j+1}, \widehat{a}_{i,j+1}, \widehat{a}^{\dagger}_{i+2,j}, \widehat{a}_{i+2,j}, \widehat{a}^{\dagger}_{i,j+2}, \widehat{a}_{i,j+2}\big),$$

where $[\widehat{a}_{i,j}, \widehat{H}]$ stands for the commutator of $\widehat{a}_{i,j}$ and $\widehat{H}$. From (4), one can obtain the equation of motion for average $\langle\Phi_{i,j}|\widehat{a}_{i,j}|\Phi_{i,j}\rangle$ as follows:

$$i\frac{d\Phi_{i,j}}{dt} = -\mu\Phi_{i,j} - t_x(\Phi_{i+1,j} + \Phi_{i-1,j}) - t_y(\Phi_{i,j+1} + \Phi_{i,j-1})$$
$$-t_x^{'}(\Phi_{i+2,j} + \Phi_{i-2,j}) - t_y^{'}(\Phi_{i,j+2} + \Phi_{i,j-2}) + \frac{U}{2}|\Phi_{i,j}|^2\Phi_{i,j}. \quad (5)$$

From the motion equation (5), let us study the stability analysis in the next section.

Stability Analysis

In this section, we investigate the stability of a constant amplitude solution of 2D ultracold atoms loaded in optical square lattices including and NNN hopping. At this stage, we first look the slow modulation of a carrier wave by considering the trial solution to the equation of motion (5) in the form:

$$\Phi_{i,j} = \Phi_0 e^{i(k_x ai + k_y bj - \omega t)}, \qquad (6)$$

where *a* and *b* stand for the lattice constants in the *x* and *y* directions, Φ_0 denotes the initial amplitude, k_x and k_y are the wavenumbers of the plane carrier wave whereas ω denotes the

frequency of the plane wave. Inserting(6) into, (5), we get the dispersion relation, which is read:

$$\omega = -\mu - 2t_x \cos(k_x a) - 2t_y \cos(k_y b) - 2t_x^{'} \cos(2k_x a) - 2t_y^{'} \cos(2k_y b) + \frac{U}{2}|\Phi_0|^2 \qquad (7)$$

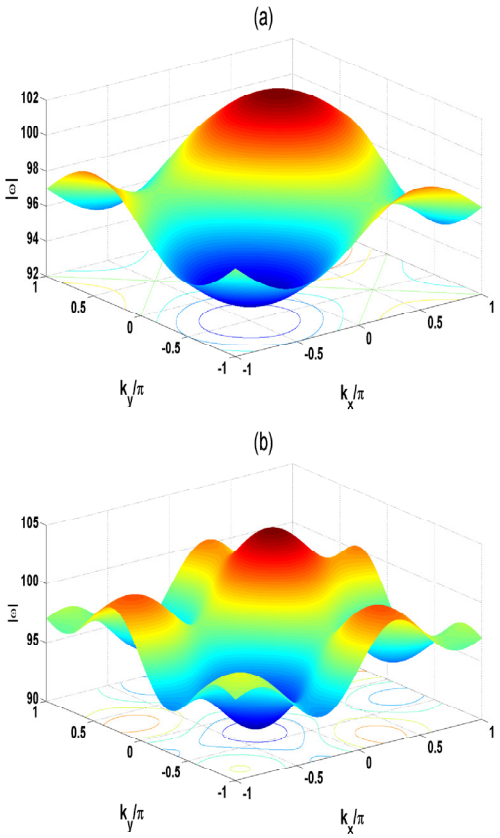

Figure 1: (Color Online) Dispersion Relation in Terms of Wave Vector. The Parameters of the Quantum Ultracold Atoms Loaded in Optical Lattices are : $t_x = t_y = 1$, $|\phi_0| = 0.2$, $a = b = 1$, $U = 150$ and (a): $t'_x = t'_y = 0$ (b): $t'_x = t'_y = 0.9$

(7)is the dispersion relation of 2D optical lattice. This dispersion relation is plotted on Figure. 1(a)-(b) for $U = 150$, in the absence of second neighbor hopping, it is shown that, the angular frequency of optical waves is minimum for certain wavenumbers as $k_x/\pi = k_y/\pi = -0.5$ at the first boundary of the Brillouin zone whereas the angular frequency is maximum for $k_x/\pi = k_y/\pi = 0.5$ at the second boundary of the Brillouin zone as depicted on Figure. 1(a). As illustrated on Figure. 1(b) for $t'_x = t'_y = 0.9$ indicating the presence of second neighbor hopping in the system, has significantly changed the shape of the angular frequency of optical waves by slightly increasing the maximum value although displaying dramatic maximum in the Brillouin zone. It is also found that, the localization of minimum and maximum of the angular frequency can change the localization in the Brillouin zone by using the attractive case of on-site interaction ($U < 0$). These cases are not presented here avoiding to overloading the paper.

Therefore, one can conclude that, the dispersion relation formed exhibits intriguing form displaying minimums and dramatic maximum of angular fre- quency at certain wavenumbers while the second neighbor hopping are in-cluded in this optical lattice. This demonstrates that, the introduction of the NNN hopping may affect the dispersion relation of the system. Therefore, we predict that the formation of instability regions will be depended on the value of second neighbor hopping and on the sign on-site interaction constant (repulsive and attractive).

Next, to evaluate criteria for propagating isolated pulses, let us adopt the perturbed nonlinear wave in the following form:

$$\Phi_{i,j} = \left[\Phi_0 + \delta\Phi_{i,j}(t)\right] e^{i(k_x ai + k_y bj - \omega t)}, \qquad (8)$$

with $\delta\Phi_{i,j}(t) \ll \Phi_0$.

Inserting (8) into (5) and keeping only the linear terms $\delta\Phi_{i,j}$ and $\delta\Phi^*_{i,j}$ as in [48]. we have a differential equation which is:

$$\begin{aligned} i\frac{d\delta\Phi_{i,j}}{dt} = &-2t_x\left[\delta\Phi_{i-1,j}e^{-ik_xa} + \delta\Phi_{i+1,j}e^{ik_xa} - 2\cos(k_xa)\delta\Phi_{i,j}\right] \\ &-2t_y\left[\delta\Phi_{i,j-1}e^{-ik_yb} + \delta\Phi_{i,j+1}e^{ik_yb} - 2\cos(k_yb)\delta\Phi_{i,j}\right] \\ &-2t'_x\left[\delta\Phi_{i-2,j}e^{-i2k_xa} + \delta\Phi_{i+2,j}e^{i2k_xa} - 2\cos(2k_xa)\delta\Phi_{i,j}\right] \\ &-2t'_y\left[\delta\Phi_{i,j-2}e^{-i2k_yb} + \delta\Phi_{i,j+2}e^{i2k_yb} - 2\cos(2k_yb)\delta\Phi_{i,j}\right] \\ &+\frac{U}{2}\left[2|\Phi_0|^2\delta\Phi_{i,j} + \Phi_0|^2\delta\Phi^*_{i,j}\right]. \end{aligned} \tag{9}$$

Moreover, we analyze the stability of the zero solution of (9) by introducing small perturbations by expressing the Fourier modes in the form :

$$\delta\Phi_{i,j}(t) = \Phi_1 e^{i(Qi+Qj-\Omega t)} + \Phi^*_2 e^{-i(Qi+Qj-\Omega t)}, \tag{10}$$

where Q and Ω denotes the wave number and the frequency of the modulated waves, respectively, whereas the asterisk indicates the complex conjugation. Φ_1 and Φ_2 are the constants amplitudes of the carrier wave.

Substituting (10) into (9), one can get the following homogenous equations for Φ1 Φ_1 and $\Phi_2$as follows:

$$\begin{cases} (\Omega - M_{11})\Phi_1 + M_{12}\Phi_2 = 0 \\ M_{21}\Phi_1 + (\Omega - M_{22})\Phi_2 = 0 \end{cases} \tag{11}$$

The condition for the existence of nontrivial solutions of (11) can be described as a second-order equation for the frequency Ω of modulated wave giving by:

$$\Omega^2 + \Big(M_{11} - M_{22}\Big)\Omega + M_{12}M_{21} - M_{11}M_{22} = 0, \tag{12}$$

with

$$\begin{aligned} M_{11} = M_{22} &= 2t_x\sin(k_xa)\sin(Q) + 2t_y\sin(k_yb)\sin(Q) \\ &+2t'_x\sin(2k_xa)\sin(2Q) + 2t'_y\sin(2k_yb)\sin(2Q) \\ M_{12} &= -4sin^2(Q/2)\left[t_x\cos(k_xa) + t_y\cos(k_yb)\right] \\ &-4sin^2(Q)\left[t'_x\cos(2k_xa) + t'_y\cos(2k_yb)\right] + \frac{U}{2}\left[|\Phi_0|^2 - \Phi_0^2\right] \\ M_{21} &= -4sin^2(Q/2)\left[t_x\cos(k_xa) + t_y\cos(k_yb)\right] \\ &+t'_x\cos(2k_xa) + t'_y\cos(2k_yb)\right] - \frac{U}{2}\left[|\Phi_0|^2 + \Phi_0^2\right]. \end{aligned} \tag{13}$$

To find the appearance condition of an instability in 2D ultracold atoms in optical lattices, let us rewrite (12) in the following form:

$$\Omega^2 = M_{11}M_{22} - M_{12}M_{21}. \tag{14}$$

From (14), it is found that, the instability will emerge in 2D optical lattices if the right-hand side of (14) is negative.

It is found that, two complex numbers are solutions of (14) if $\Omega^2 < 0$. The exponential growth of perturbation is represented by the MI gain. In this circumstance, the MI power gain spectrum gain(G) of the system known as growth rate, can be expressed by using the following formula as in references [49,21]:

$$gain(G) = Im(\Omega). \tag{15}$$

The first study has been realized to show the development of the MI in 2D quantum ultracold atoms loaded in optical lattices including first nearest neighbors [36]. Without harming the generality, the effects second neighbor hopping and on-site interaction are displayed on Figure. 2 showing a manifestation of the MI spectrum in the optical lattices for different values of $t'_x = t'_y$, controlling the coupling interactions between nearest-neighbor and second neighbor

hopping in 2D ultracold atoms in optical lattices for the repulsive case for

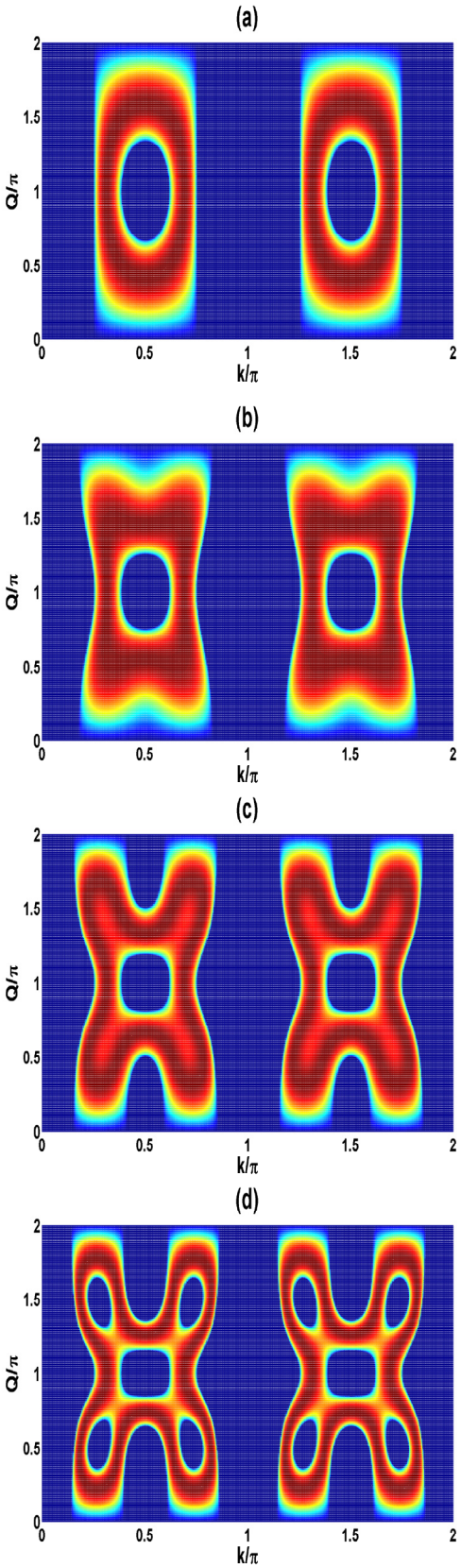

Figure: 2 (Color Online) Stability/Instability Regions on the (k,Q) Plane for Different Value the Hopping Second Neighbors Amplitudes where $a = b = 2$, $k_x = k_y = k$, $|\phi_0| = 0.2$, $U = 150$ and $t_x = t_y = 1$; (a) $t'_x = t'_y = 0$ (b): $t'_x = t'_y = 0.2$, (c): $t'_x = t'_y = 0.5$ and (d): $t'_x = t'_y = 0.9$

U = 150, depicting the stability/instability diagrams in the (k,Q) plane. It is shown on these diagrams that; the dark bluish area regions illustrate zones of stability whereas regions with bright yellowish orange area indicate the zone of instability. In the absence of second-neighbor hopping in optical lattices, the instability regions which clearly appear in the Brillouin zone especially for k/π = 0.5 and k/π = 1.5, display two symmetric uniform rectangular shapes, each of them exhibiting a circular stability area located at the center of each sideband as exhibited on Figure.2(a). Similar results

have been obtained in where, it was demonstrated that, an increasing value of repulsive interaction may increase the shape and the amplitude of the region of instability [36]. However, by increasing the value of second neighbor hopping coupling strength to 0.2, leads to an increase the width of the instability region and to deform its shape and the stability areas with circular form as changed into square one as presented on Figure.2(b). As we increase the value of second neighbor hopping range to 0.5, an appreciable new shape of the instability region like a star is observed on Figure.2(c). By increasing the value of second neighbor hopping coupling strength to 0.9, it is clearly observed on Figure.2(d) that, the previous shape of instability region like a star remains with the difference that, this new shape displays 5 zones of stability in star of the one with square form previously shown on Figure.2(c).

Figure.3(a)-(d) depicts the 3D plot of MI gain in the (k, Q) plane for different values second neighbor hopping coupling strength showing, the effects of coupling interaction on appearance of MI regions in this 2D quantum ultracold atoms loaded in optical lattices described in Figure.2 where, it is shown that, the emergence of MI regions can be controlled by the coupling interaction lying first and second nearest neighbors. Nevertheless, the peaks remain uniform in amplitude appear to remain the same. This can be justified by the fact that; the value of the on-site interaction has not changed.

Further, by changing the sign of the on-site interaction to negative to obtain the attractive case, it is clearly shown in Figure.4 (a) that, the MI regions emerge at the center and at the end of the Brillouin zone by displaying rectangular sidebands. Similar results have been reporter in the absence of second neighbors hopping with the difference that, in the present case, the lattice spacing constant is set to 2 ($a = b = 2$) instar of 1 [36].

In the presence of second nearest neighbors, when the second neighbors hopping coupling strength is low ($t'_x = t'_y = 2$), although the sidebands remain symmetric, as we can observe on Figure.4 (b), its shape has significantly modified by exhibiting hexagonal feature. However, when this parameter becomes average and set to 0.5, the number of sidebands remains identical by keeping their hexagonal shape and separated by four new regions of MI which appear on the MI spectrum as illustrated on Figure.4 (c). For the strong values of coupling strength ($t'_x = t'_y 9$), it is shown on Figure.4 (d) that, the strong second neighbors hopping has for effect to significantly increase the width of four new regions of the MI slightly observed on Figure.4 (c).

The 3D plot of MI gain of this on-site attractive case is depicted on Figure.5, with the difference that, the amplitude of four lobes pointed out on Figure.5

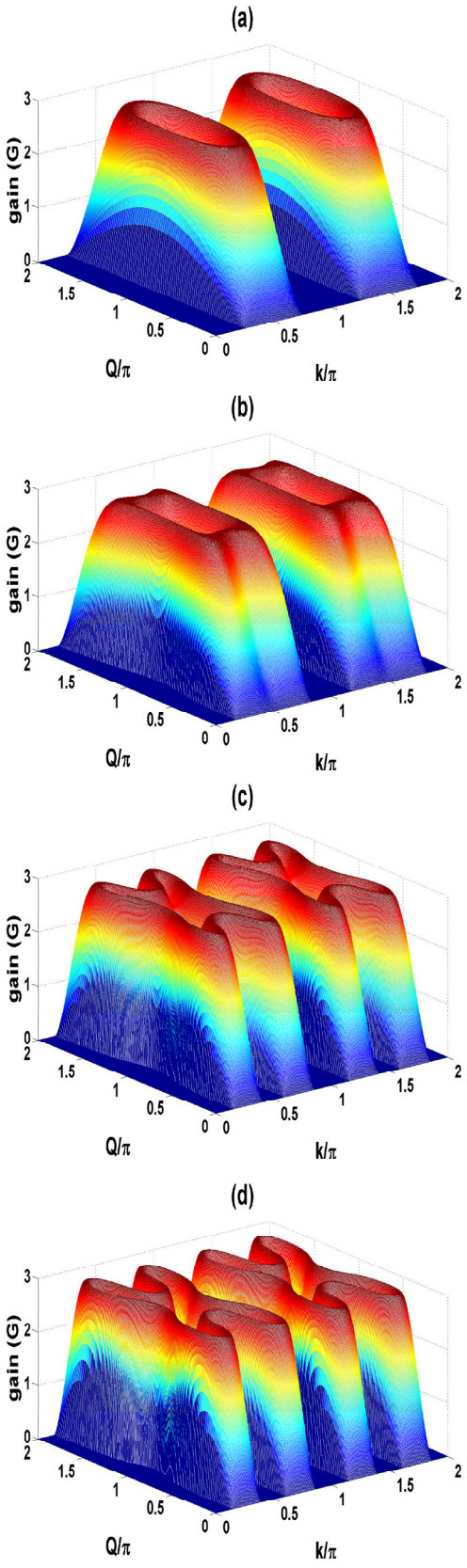

Figure 3: (Color Online) Instability Gain Plotted in 3D with the Same Parameters Used in Figure. 2

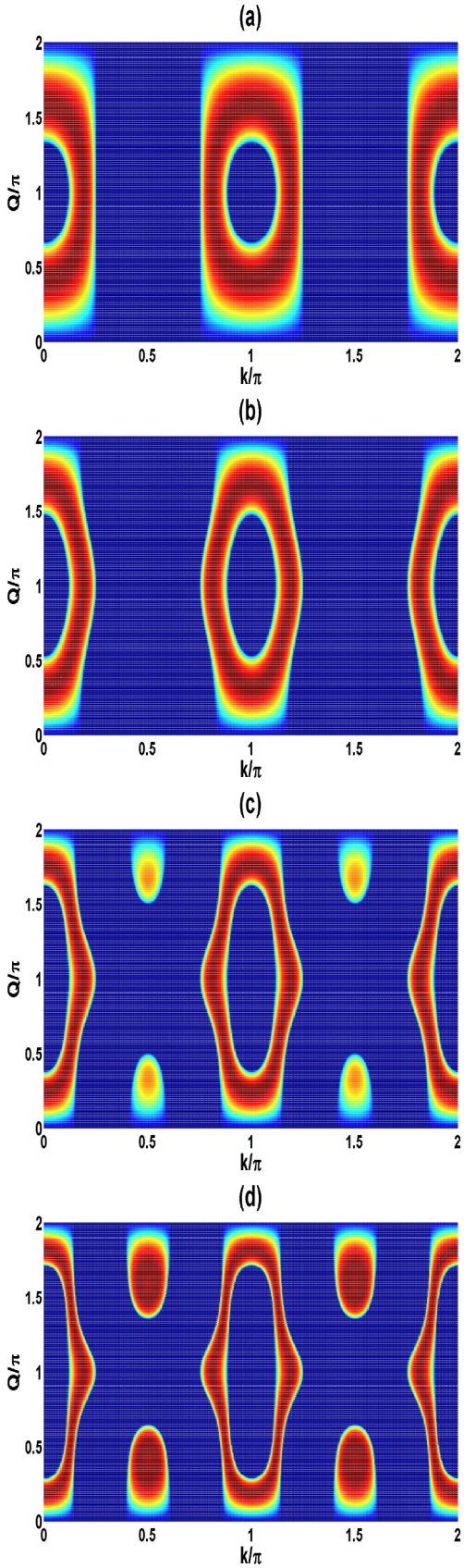

Figure 4: (Color Online) Stability/Instability Regions on the (K,Q) Plane for Different Value the Second Neighbors Interactions where $a = b = 2$, $k_x = k_y = k$, $|\phi_0| = 0.2$, $U = -150$ and $t_x = t_y = 1$; (a): $t'_x = t'_y = 0$ (b): $t'_x = t'_y = 0.2$, (c): $t'_x = t'_y = 0.5$ and (d): $t'_x = t'_y = 0.9$

(c) is reduced comparing to the case presented on Figure.5 (d) when the second neighbors hopping becomes high.

Considering the values of the on-site interaction $U = \pm 1500$, these cases are presented on Figure.6 and Figure.7, respectively where the unstable zones clearly manifest by displaying two dominated side lobes containing five small peaks with uniform amplitude as pointed out in Figure.6(a)-(b) for $U = 1500$, with the difference that, the amplitude is increased than in the previous cases for which the on-site interaction values were low. The attractive case is shown on

Figure.7(a)-(b), where the instability aperture exhibits three side lobes each of them containing two peaks on top which appears to be a bit broadened than in the previous case shown on Figure.5.

From Figure.3, 5, 6, 7, it is clearly noted that, there are some values of Q and k known as marginal instability points for which, the growth rate of the MI is maximal. To check this, we have portrayed on Figure.8, the growth rate spectra as a function of the wavenumbers Q of perturbation. In this way, let us start by considering the repulsive case (U = 150) for different values of coupling interaction plotted with solid black line, dotted blue line and red solid line. For $Q = \pi/4$, plotted on Figure. 8(a) demonstrating that, the intensity of the growth rate of MI increases with an increasing value of second neighbor hopping, while the bandwidths in the absence of second neighbor hopping are large and symmetric (see solid black line). Each initial bandwidth in solid black line is splitting into two sidebands for $t'_x/t_x = t'_y / t_y = 0.5$ as illustrated with dotted blue line. However, for $t'_x/t_x = t'_y / t_y = 0.9$, the bandwidth practically remains constant as in the case with blue line with the difference that its marginal instability point displays four peaks and confirms our prediction made on Figure.3.

Next, for $Q = 3\pi/4$, the dependence of the magnitude of the growth rate and MI bandwidth presents the inverse behavior when comparing with the case shown Figure.8(a) with the difference that, the marginal instability point is constant and remains unchanged while the second neighbor hopping are included in the system. For instance, in the absence of second neighbor hopping as presented with the back solid line curve on Figure.8(b), each bandwidth is spitted into two bands whereas in the presence of second neighbor hopping illustrated by blue curve with two large bandwidths displaying each of them two maximums and one minimum. These two large bandwidths slightly increase by exhibiting each of them three maximums and two minimums when the coupling interaction is high as presented with red curve which confirms our prediction made on Figure.3. We can therefore infer that; the magnitude of the growth rate and the bandwidth depend on the best choice of the value of wavenumber of perturbation Q and can be fully controlled by the second nearest neighbors coupling.

In the case of attracting on-site interaction, for $Q = \pi/4$, the intensity of the growth rate of MI is low with periodic bandwidth in the absence of second neighbor hopping as presented by the black solid line on Figure.9(a). In the presence of second neighbor hopping, the marginal instability point is obtained and the number of periodic bandwidths increases when the coupling interaction is strong (see curves with blue and red line) and valid our prediction made on Figure.5. For $Q = 3\pi/4$, it is clearly shown on Figure.9(b) that, the width of the bandwidth decreases with the presence of second neighbor hopping.

By taking the fact that, the linear stability analysis cannot give more information of the long-time evolution of a modulated nonlinear wave, to examine the validity of a linear stability analysis results, the numerical analysis of MI will be investigated in the next section through direct numerical integrations of (5).

Numerical Analysis

We put our analytical predictions against the unyielding challenge of direct numerical simulations on (5). In this way, to achieve our aim, we use a fourth order Runge Kutta algorithm, a time step chosen to an accuracy better than 5×10^{-3} in the initial condition which is a modulated plane wave expresses as in [21,49]:

$$\Phi_{i,j}(t=0) = \Phi_{0,0}\Big[1+\beta\cos(Qia+Qjb)\Big] \times \cos\big(k_x ia + k_y jb\big), \qquad (16)$$

where $\Phi_{0,0}$ is set to 0.5, β = 0.01 is the modulation index. The simulations have been performed in the lattice with the size 400 × 400 sites, with periodic boundary conditions by assuming that the wavenumbers $k(k_x,k_y)$ and $Q(Q_x,Q_y)$ must necessarily to be in the form $k = k_x = k_y = 2\pi l/N$ and $Q = Q_x = Q_y = 2\pi L/N$, with l and L integers but lower than $N/2$.

When the initial condition (16) is introduced numerically into (5), by choosing for example, a couple of points in the (k,Q) plane lying the instability domain obtained in Figure.2. In the absence of second neighbor hopping meaning that, the coupling strength is nil ($t'_x = t'_y = 0$), with a couple of points ($k = 5\pi/100, Q = 2\pi/10$) where the corresponding point lies in an instability region of Figure.2(a). This case is plotted on Figure.10 at various time stages.

Let us start by the first time stage. At $t = 0$, the initial modulated wave exhibits a periodic oscillating behavior as shown on panel (a1) plotted in 3D and (c2) his corresponding amplitude projected in the $i = j$ plane displaying periodic V-shaped profile with a constant amplitude. The modulus of this modulated wave displays new feature, showing that the disintegrated wave leads to the break-up of waves into localized patterns with high amplitude where each element of the train looks like a soliton object as presented in panel (c1).

Next, at t = 50, as we can observe on panel (a2), the initial modulated wave during its propagation is disintegrated and has changed its shape into a train like-object whereas his corresponding amplitude is very decreased during this propagation by displaying the breathing behavior with constant amplitude in panel (c2). By comparing with case on panel (c1), it is noted that this amplitude gradually decreases over the time. The panel (b2) shows that, the number of

waves train increases with time, but the maximum amplitude is decreased than the case shown on panel (b1).

Finally, at t = 100, new feature is observed on panel (a3) indicating that the modulated wave as the time progresses is gradually disintegrated by changing his shape into a train like-object whereas his corresponding amplitude is dramatically decreased by exhibiting an anti-symmetric V-shaped soliton profile in panel (c3). However, his modulus has also changed the shape and the number of waves train is dramatically reduced.

From Figure.12, we note the amplitude intensity of the modulated wave decreases as the time increases, its shape changes over time and his modulus for a long-time evolution generates new features of solitonic wave structure.

These results confirm once again the fact that, the linear stability analysis cannot give more information of the long-time evolution of a modulated nonlinear wave. This can be justified by the fact that as the time increases, the modulated wave changes it shape and validates the instability modulated wave during its propagation. Such investigations have been shown in 2D MI [50].

To study the influence of second neighbors hopping, we have set the coupling strength as $t'_x = 0.9t_x$ and $t'_y = 0.9t_y$. In this case, the propagation of the modulated wave is portrayed on Figure.13 at various time stages as in the previous case as follows.

At t = 0, the initial modulated wave exhibits a periodic oscillating behavior as shown on panel (a1) with his corresponding amplitude projected in the $i = j$ plane displaying V-shaped periodic profile with a constant amplitude as we can see on panel (c1) whereas his modulus is disintegrated into train of high amplitude waves and presented on panel (b1).

Surprisedly, at t = 50, it is shown on panel (a2) of Figure.13 that, the initial modulated wave during its propagation has changed the shape by presenting a new feature of oscillating wave with very small amplitude like a train of short waves exhibiting periodic W-shaped solitons as illustrated on panels (b2)-(c2). These excitations are very stable, can travel without changing their shape and are important in the coherent transfer of energy. As the time involves, the amplitude of the modulated wave dramatically decreases. This leads to conclude that, the inclusion of second neighbor hopping in the optical lattice may influence the formation of solitonic structures over time.

At t = 100, new features with slight fluctuations appear on panels (a3), (b3) and (c3) and their amplitude gradually decrease as the time evolves.

From Figure.13, which confirms the fact that, the plane wave is sensitive to any value of second neighbors hopping, it is noted that, the modulated wave patterns manifesting the modulation instability with the inclusion of second neighbor hopping. This implies that, the formation of solitonic structures can be controlling by the second neighbor hopping.

Therefore, confirming hypothesis for which, the plane wave is sensitive to any value of the wavenumber, we have seen that the couple of points chosen which lies the instability region as example to propagate the modulated wave, manifests the modulation instability of the system and therefore validates the linear stability analysis.

To check the validity of analytical results, we adopt the semi-discrete approximation and multiple-scale method of Remoissenet to transform (5) into a nonlinear Schr¨odinger equation in the next section [51].

Semi-Discrete Approximation and Multiple-Scale Method Applied in 2D Ultracold Atoms Model

We attempt in this section to construct approximations to small amplitude of (5), the semi-discrete approximation and multiple scale asymptotic techniques are used. We introduce new variable defined by:

$$\Phi_{i,j} = \varepsilon\phi_{i,j}, \tag{17}$$

where ϵ stands for a small finite parameter. Inserting (17) into (5) leads to

$$\begin{aligned} i\frac{d\phi_{i,j}}{dt} &= -\mu\phi_{i,j} - t_x(\phi_{i+1,j} + \phi_{i-1,j}) \\ -t_y(\phi_{i,j+1} + \phi_{i,j-1}) &- t'_x(\phi_{i+2,j} + \phi_{i-2,j}) \\ -t'_y(\phi_{i,j+2} + \phi_{i,j-2}) &+ \varepsilon^2\frac{U}{2}|\phi_{i,j}|^2\phi_{i,j}. \end{aligned} \tag{18}$$

To get the solution of (18), it is important to restrict ourselves to the wave which, consists of a slowly varying envelope solution by modulating a car- rier wave. These methods applied to soliton equations demonstrated by Re- moissenet [52]. For sake of simplicity, we shall use a simplified version of multiple-scale technique, by considering the space and time scale are new variables set to : $x_j = \varepsilon^j x,\ y_j = \varepsilon^j y$ and $t_j = \varepsilon^j t$, where x_j , y_j and t_j stand for independent variables. The derivative independent operators variables for spatial derivative d/d_x, d/d_y and for time derivative d/dt can be evaluated as:

$$\frac{d}{dx} = \frac{\partial}{\partial x_0} + \varepsilon\frac{\partial}{\partial x_1} + \varepsilon^2\frac{\partial}{\partial x_2} + \cdots, \qquad (19)$$
$$\frac{d}{dy} = \frac{\partial}{\partial y_0} + \varepsilon\frac{\partial}{\partial y_1} + \varepsilon^2\frac{\partial}{\partial y_2} + \cdots,$$
$$\frac{d}{dt} = \frac{\partial}{\partial t_0} + \varepsilon\frac{\partial}{\partial t_1} + \varepsilon^2\frac{\partial}{\partial t_2} + \cdots,$$

with $x_j(x_1 = \epsilon x, x_2 = \epsilon^2 x, \ldots)$, $y_j(y_1 = \epsilon y, y_2 = \epsilon^2 y, \ldots)$ and $t_j(t_1 = \epsilon t, t_2 = \epsilon^2 t, \ldots)$ where $\epsilon << 1$ being the small amplitude of the breather and the variables x_j , y_j will be behaved as continuous real variables. Taking into account these derivatives given in (19), the modulated wave solution can be written in the form:

$$\phi_{i,j} = \psi_{i,j}(t_1, t_2, x_1, y_1)\exp(i\theta_{i,j}), \qquad (20)$$

where $x_1 = \varepsilon ia = \varepsilon x$, $y_1 = \varepsilon jb = \varepsilon y$, a and b are lattice constants, $\theta_{i,j} = k_x ia + k_y jb - \omega t$ is the phase, k the wave number of the linear carrier wave and ω denotes the frequency of the carrier wave.

Next, inserting(19) and (20) into (18), we derive the following nonlinear differential equation which is:

$$\begin{aligned}
&\Big[\omega + \mu + 2\big(t_x\cos(k_x a) + t_y\cos(k_y b)\big) + 2\big(t_x^{'}\cos(2k_x a) + t_y^{'}\cos(2k_y b)\big)\Big]\psi_{i,j}e^{i(\theta_{i,j})} \\
&+i\varepsilon\Big[\tfrac{\partial\psi_{i,j}}{\partial t_1} + 2a\big(t_x\sin(k_x a) + 2t_x^{'}\sin(2k_x a)\big)\tfrac{\partial\psi_{i,j}}{\partial x_1} \\
&+2b\big(t_y\sin(k_y b) + 2t_y^{'}\sin(2k_y b)\big)\tfrac{\partial\psi_{i,j}}{\partial y_1}\Big]e^{i(\theta_{i,j})} \\
&+\varepsilon^2\Big\{i\tfrac{\partial\psi_{i,j}}{\partial t_2} + a^2\Big(t_x\cos(k_x a) + 4t_x^{'}\cos(2k_x a)\Big)\tfrac{\partial^2\psi_{i,j}}{\partial x_1^2} \\
&+b^2\Big(t_y\cos(k_y b) + 4t_y^{'}\cos(2k_y b)\Big)\tfrac{\partial^2\psi_{i,j}}{\partial y_1^2} - \tfrac{U}{2}\big|\psi_{i,j}\big|^2\psi_{i,j}\Big\}e^{i(\theta_{i,j})} \\
&+O(\varepsilon^3) = 0.
\end{aligned} \qquad (21)$$

By setting the coefficient of powers " to zero in Eq.(21), we get the following equations:

$$\begin{aligned}
\omega + \mu + 2\big(t_x\cos(k_x a) + t_y\cos(k_y b)\big) + 2\big(t_x^{'}\cos(2k_x a) + t_y^{'}\cos(2k_y b)\big) &= 0, \\
\frac{\partial\psi_{i,j}}{\partial t_1} + 2a\Big(t_x\sin(k_x a) + 2t_x^{'}\sin(2k_x a)\Big)\frac{\partial\psi_{i,j}}{\partial x_1} + 2b\Big(t_y\sin(k_y b) + 2t_y^{'}\sin(2k_y b)\Big)\frac{\partial\psi_{i,j}}{\partial y_1} &= 0, \\
i\frac{\partial\psi_{i,j}}{\partial t_2} + a^2\Big(t_x\cos(k_x a) + 4t_x^{'}\cos(2k_x a)\Big)\frac{\partial^2\psi_{i,j}}{\partial x_1^2} + b^2\Big(t_y\cos(k_y b) + 4t_y^{'}\cos(2k_y b)\Big)\frac{\partial^2\psi_{i,j}}{\partial y_1^2} & \\
-\frac{U}{2}\big|\psi_{i,j}\big|^2\psi_{i,j} &= 0.
\end{aligned} \qquad (22)$$

It is easy to deduce from the dispersion relation of the system given in (22) its group velocity given by:

$$v_g = \Big(v_{gx} = 2t_x a\sin(k_x a) + 4at_x^{'}\sin(2k_x a), v_{gy} = 2t_y b\sin(k_y b) + 4t_y^{'}b\sin(2k_y b)\Big). \qquad (23)$$

From (22), we note that spatial and time derivatives of envelope function are closely connected. This means that they depend on each other as expected. This envelope function can be regarded as a traveling wave form which is can be expressed as

$$\psi_{i,j}(t_1, t_2, x_1, y_1) = \psi_{i,j}(\tau_2, z_{1x}, z_{1y}), \qquad (24)$$

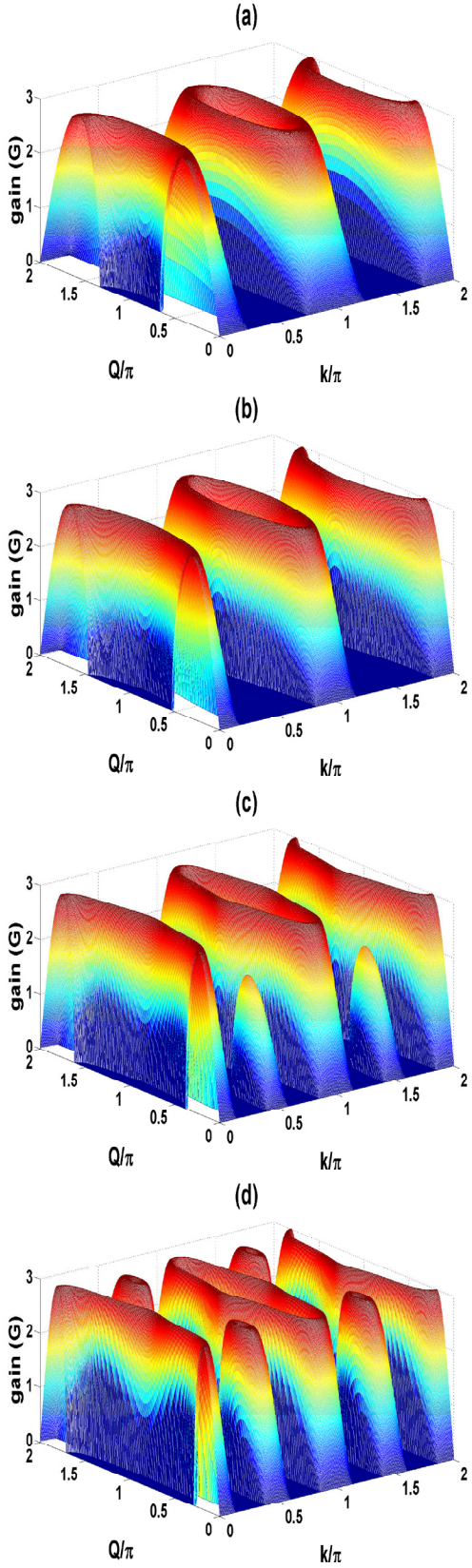

Figure: 5 (Color Online) Instability Gain Plotted in 3D with the Same Parameters Used in Figure.4

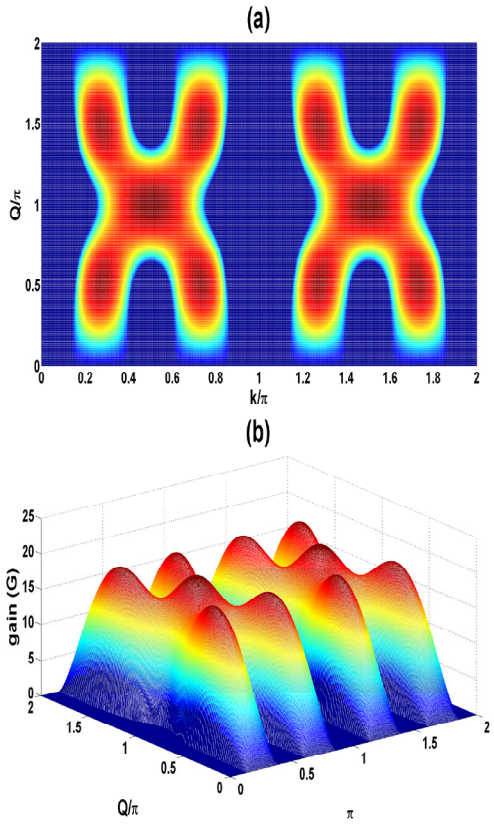

Figure: 6 (Color Online) Stability/Instability Regions on the (k,Q) Plane and Instability Gain In Repulsive Case for $a = b = 2$, $k_x = k_y = k$, = 0.2, $U = 1500$, $t_x = t_y = 1$ and 9; (a): Stability/Instability Regions (b): Instability Gain

where, the new scale introduced are $z_{1x} = x_1 - v_{gx}t_1,\ z_{1y} = x_1 - v_{gy}t_1$. With the aid of these transformations, (22) takes the following form

$$i\frac{\partial\psi_{i,j}}{\partial t_2} + a^2\Big(t_x\cos(k_x a) + 4t_x^{'}\cos(2k_x a)\Big)\frac{\partial^2\psi_{i,j}}{\partial z_{1x}^2} \qquad (25)$$
$$+b^2\Big(t_y\cos(k_y b) + 4t_y^{'}\cos(2k_y b)\Big)\frac{\partial^2\psi_{i,j}}{\partial z_{1y}^2} - \frac{U}{2}|\psi_{i,j}|^2\psi_{i,j} = 0.$$

Making use of the following transformations $z_{1x} = \varepsilon z_x,\ z_{1y} = \varepsilon z_y,\ \psi_{i,j} = \Gamma/\varepsilon,$ and considering that $t_2 = \varepsilon^2 t,$

(??)

$$z_{1x} = a\sqrt{\frac{t_x\cos(k_x a) + 4t_x^{'}\cos(2k_x a)}{P}}z_x \qquad (26)$$

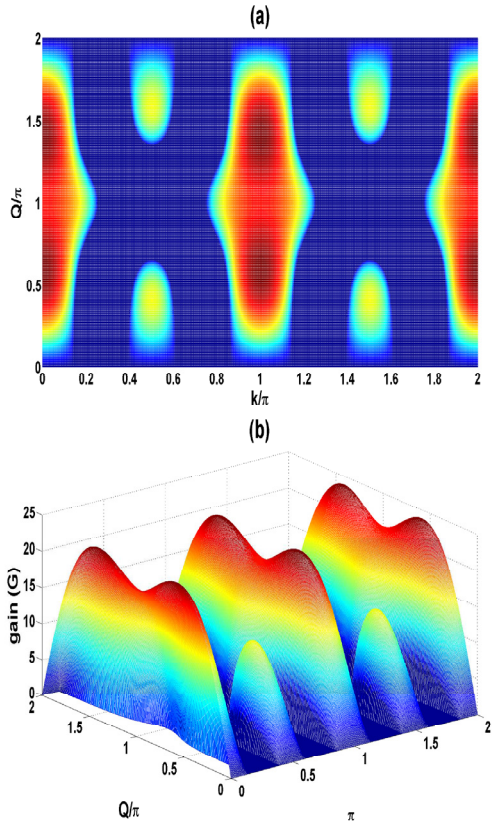

Figure: 7 (Color Online) Stability/Instability Regions on the (k,Q) Plane and Instability Gain in the Attractive Case for $a = b = 2$, $k_x = k_y = k$, $|\phi_0| = 0.2$, $U = -1500$, $t_x = t_y = 1$ and 9; (a): Stability/Instability Regions (b): Instability Gain

$$z_{1y} = a\sqrt{\frac{t_y \cos(k_y a) + 4t'_y \cos(2k_y a)}{P}} z_y,$$

(25) becomes :

$$i\frac{\partial \Gamma}{\partial t} + P\left(\frac{\partial^2}{\partial z_x^2} + \frac{\partial^2}{\partial z_y^2}\right)\Gamma + Q|\Gamma|^2\Gamma = 0, \qquad (27)$$

with $P = a^2[t_x \cos(k_x a) + 4t'_x \cos(2k_x a)] + b^2[t_y \cos(k_y b) + 4t'_y \cos(2k_y b)]$, and $Q = -U/2$.

By introducing the Laplacian operator, which describes spatial temporal dynamics of the wave packet envelope in the transverse plane (x, y), (27) can take the following form :

$$i\Gamma_t + P\triangle_\perp \Gamma + Q|\Gamma|^2\Gamma = 0, \qquad (28)$$

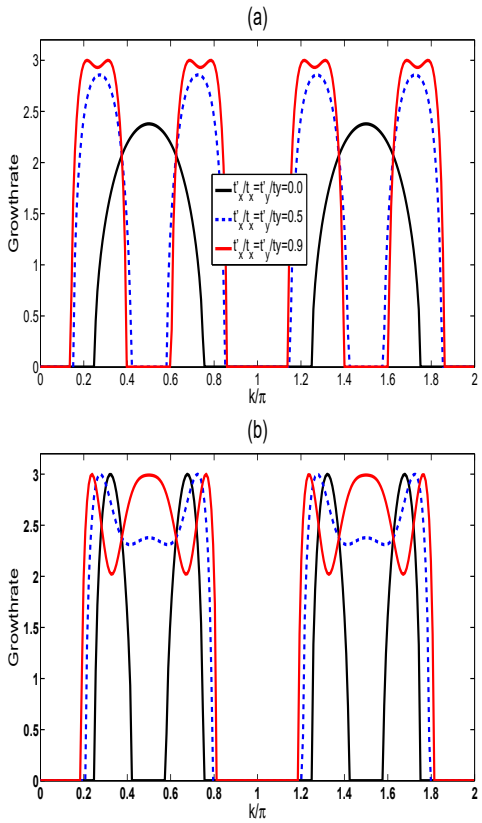

Figure: 8 (Color Online) Growth Rate of MI Versus the Wave Numbers of Perturbation Q for Different Values of Coupling Interaction in the Repulsive Case. The Main of Parameters are U = 150, a = b = 2, and $|\phi_0|2$ = 0.2: (a) Q = π/4; (b) Q = 3π/4

with $\triangle_{\perp} = \frac{\partial^2}{\partial z_x^2} + \frac{\partial^2}{\partial z_y^2}$ denotes a 2D perpendicular Laplacian operator.

(28) is called the 2D nonlinear Schrodinger equation (NLSE) containing a cubic nonlinearity where its solution depends on the sign of the product PQ. Only the case for PQ > 0 shall be considered in this study.

To understand the dynamics of breathers in this work, we shall use the Rayleigh-Ritz variational method to solve (28) in the next section.

Dynamics of Discrete Breathers

The dynamics of breathers is investigated in this section by making use of Rayleigh-Ritz variational method as defined in [53]. To reach this aim, the

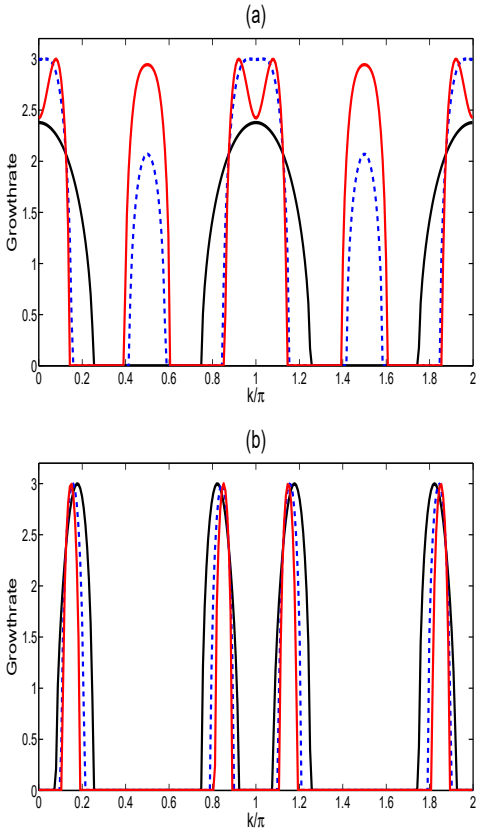

Figure: 9 (Color Online) Growth Rate of MI Versus the Wave Numbers of Perturbation Q for Different Values of Coupling Interaction in the Attractive Case. The Main of Parameters are $U = -150$, $a = b = 2$, and $|\phi_0|2 = 0.2$: (a) $Q = \pi/4$; (b) $Q = 3\pi/4$

solution of Eq.(28) is found in the form:

$$\Gamma = \exp(i\mu t)\psi(r), \tag{29}$$

where $r = \sqrt{z_x^2 + z_y^2}$.

Substituting (29) into (28) leads to the following equation with a variational structure which is:

$$-\mu\psi + P\nabla^2\psi + Q\psi^3 = 0, \tag{30}$$

with $\nabla^2 = \frac{\partial^2}{\partial z_x^2} + \frac{\partial^2}{\partial z_y^2}$.

Considering the fact that (30) has a variational structure and therefore taking its action integral ξ as a function of ψ which is given by:

$$\xi(\psi) = \int \left(\frac{1}{2}\mu|\psi|^2 + \frac{1}{2}P|\nabla\psi|^2 - \frac{1}{4}Q|\psi|^4\right)dS, \tag{31}$$

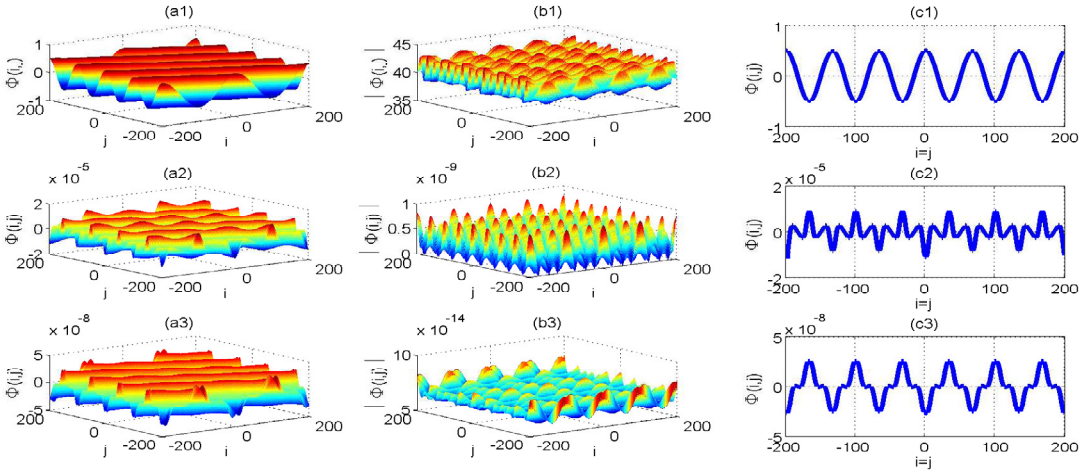

Figure. 10 (Color Online) Propagation of the Perturbed Plane Wave Intensity Without the Second Nearest Neighbor Interaction for Various Time Stages in the Attractive Case. the main of parameters are 10),$Q_x = Q_y = 5\pi/100$: 1- At the initial time $t = 0$; 2- At time $t = 50$, and 3- At the Final time $t = 100$. The Left Column is the 3D Plot, the Middle the Modulus, and the Right is the Projection in $i = j$ Plane

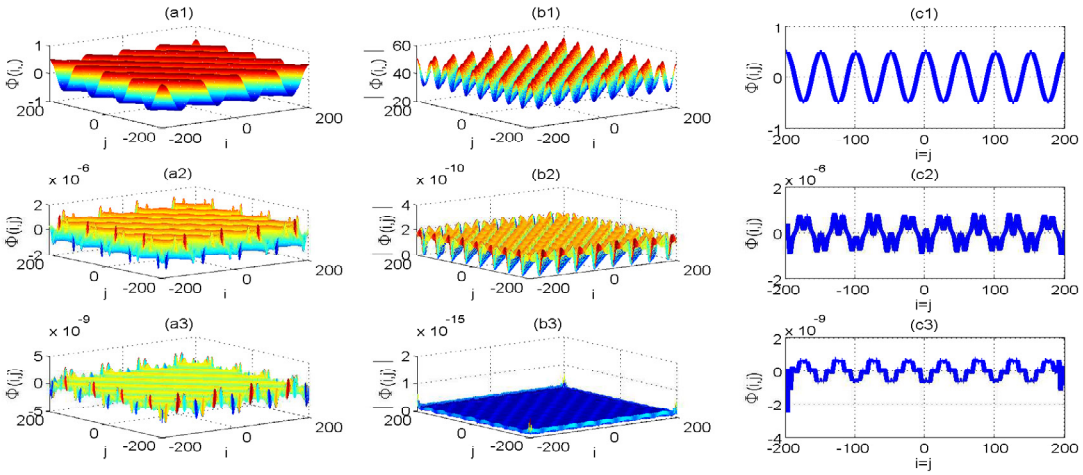

Figure: 11 (Color Online) Propagation of the Perturbed Plane Wave Intensity and Manifestation of the MI Under the Influence of the Second Nearest Neighbor Coupling for Various Time Stages in the Attractive Case. The Main of Parameters are $U = 150$, $a = b = 2$, $|\phi_0|2 = 0.2$, $t_x = t_y = 1$, $t_x = t_y = 0$, $k_x = k_y = 2\pi/10$), $Q_x = Q_y = 5\pi/100$: 1- At the initial time $t = 0$; 2- At time $t = 50$, and 3- At the final time $t = 100$. The Left Column is the 3D Plot, The Middle the Modulus, and the Right is the Projection in $i = j$ Plane

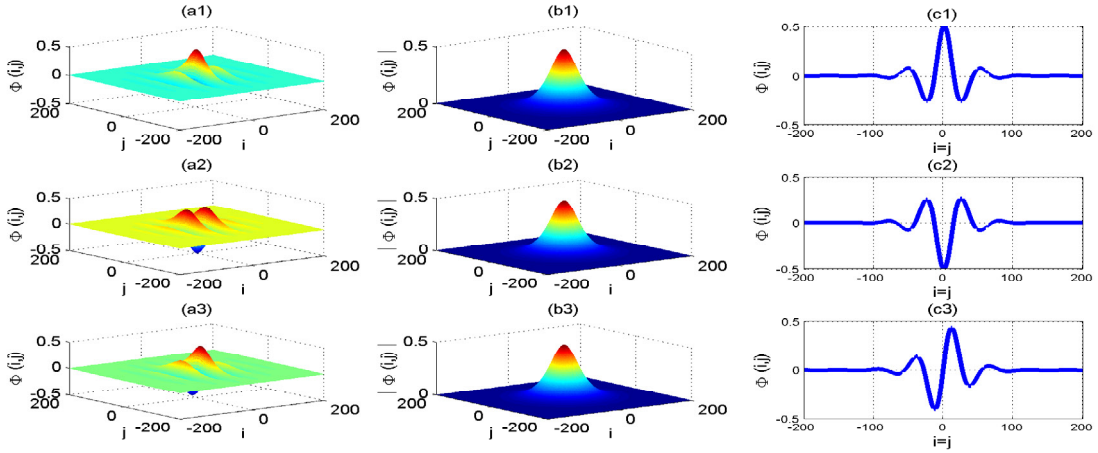

Figure: 12 (Color Online) Time Evolution of the Coherent Amplitude Φ(i,j) Obtained by Solving the Discrete NLS Eq.(5) for Values of Wave Number ($k_x = \pi/55, k_y = \pi/55000$). The Initial Wave Form is Taken as Given in Eq. (41) With Initial Amplitude.The Remaining Parameters are : 1- At the initial time $t = 0$; 2- At time $t = 50$, and 3- At the final time $t = 100$. The Left Column is the 3D plot, the Middle The Modulus, and the Right is the Projection in $i = j$ Plane

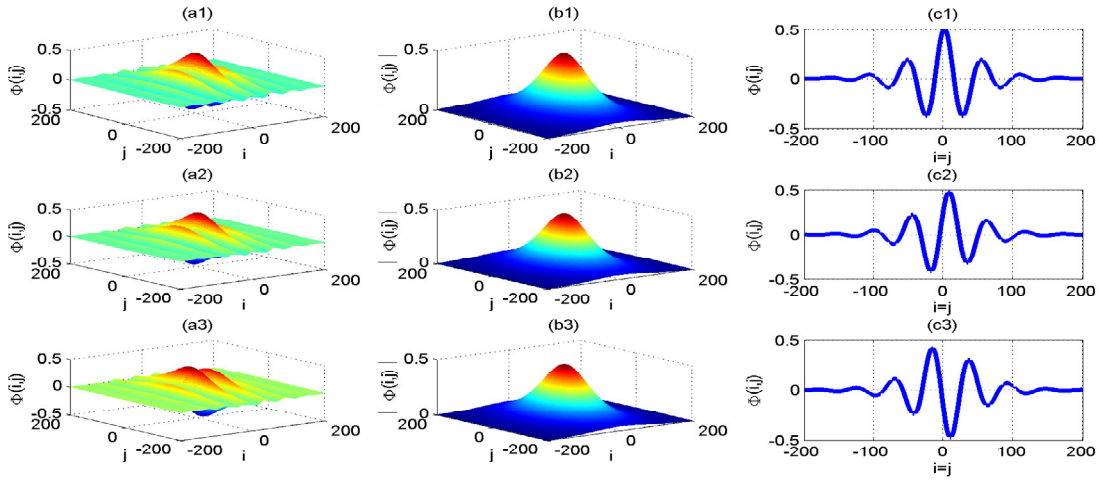

Figure: 13 (Color Online) Time Evolution of the Coherent Amplitude Φ(i,j) Obtained by Solving the Discrete NLS Eq.(5) for Values of Wave Number (k_x = π/55,k_y = π/55000). The Initial Wave Form is Taken as Given in Eq. (41) with initial amplitude . The Remaining Parameters are : 1- At the initial time t = 0; 2- At time t = 50, and 3- At the final time t = 100. The Left Column is the 3D plot, the Middle the Modulus, and the Right the Projection in $i = j$ Plane

where $dS = 2\pi r dr$, $0 < r \leq \infty$.

Depending on the sign of product PQ, (30) can admit bright and dark solutions. For $PQ > 0$, the solution is called radial bright which is

$$\psi(r) = \eta sech(\gamma r), \tag{32}$$

where η and γ denote parameter to be evaluated. Substituting (32) into (31) and evaluating numerically the resulting integral, one can obtain:

$$\xi(\eta,\gamma) = \pi\Big[\frac{P(1+2\ln 2)}{6}\eta^2 - \frac{Q(4\ln 2-1)}{12}\frac{\eta^4}{\gamma^2} + \mu \ln 2\frac{\eta^2}{\gamma^2}\Big]. \tag{33}$$

By taking into account the fact that the soliton solution corresponds to a stationary point of the action $\xi(\eta, \gamma)$, in this way, η and γ can be evaluated by using the following equation:

$$\frac{\partial\xi(\eta,\gamma)}{\partial\eta} = \frac{\partial\xi(\eta,\gamma)}{\partial\gamma} = 0. \tag{34}$$

To determine η, we differentiate $\xi(\eta, \gamma)$ with respect to γ, after that solve an equation for η^2 to find η. Once η is found, γ is determined by solving equation $\frac{\partial\xi(\eta,\gamma)}{\partial\eta} = 0$ to derive η and γ which are given by:

$$\eta = \sqrt{\frac{12\mu\ln 2}{Q(4\ln 2-1)}} \tag{35}$$

$$\gamma = \sqrt{\frac{6\mu\ln 2}{P(1+2\ln 2)}},$$

where μ is a positive constant. Let us rewrite the condition (35) as:

$$\mu = \frac{1}{12}\Big(4 - \frac{1}{\ln 2}\Big)Q\eta^2, \tag{36}$$

$$\gamma = \eta\sqrt{\frac{Q(4\ln 2-1)}{2P(1+2\ln 2)}},$$

with the constraint $PQ > 0$. Inserting (36) into (32) and substituting the result into (29) for $PQ > 0$, we obtain the time-harmonic bright radially symmetric solution in the form:

$$\Gamma = \eta \exp(i\mu t) sech\Big[\gamma\Big(\sqrt{z_x^2 + z_y^2}\Big)\Big]. \tag{37}$$

Making use of (26), we have:

$$\psi_{i,j} = \eta \exp(i\mu t_2) sech\left[\gamma\sqrt{P}\sqrt{\frac{z_{1x}^2}{A} + \frac{z_{1y}^2}{B}}\right], \tag{38}$$

where $A = a^2(t_x \cos(k_x a) + 4t_x^{'} \cos(2k_x a))$, $B = b^2(t_y \cos(k_y b) + 4t_x^{'} \cos(2k_y b))$ $z_{1x} = x_1 - v_{gx}t_1$ and $z_{1y} = y_1 - v_{gy}t_1$ are given in (24). Considering these transformations and taking into account the relation between $\psi_{i,j}$ and the modulated wave $\phi_{i,j}$ obtained in (20), Eq.(38) becomes:

$$\phi_{i,j} = \eta \exp\left(i(\theta_{i,j} + \mu t_2)\right) sech\left[\gamma\sqrt{P}\sqrt{\frac{(x_1 - v_{gx}t_1)^2}{A} + \frac{(y_1 - v_{gy}t_1)^2}{B}}\right]. \tag{39}$$

Next, replacing μ, γ and (17) by their new values given in (36), we get then:

$$\Phi_{i,j} = \eta \exp\left[i\Big(\theta_{i,j} + \frac{1}{12}\Big(4 - \frac{1}{\ln 2}\Big)Q\eta^2 t\Big)\right] sech\left[\Gamma_0\sqrt{\Upsilon\Big(\frac{(x_1 - v_{gx}t_1)^2}{A} + \frac{(y_1 - v_{gy}t_1)^2}{B}\Big)}\right], \tag{40}$$

where $\Gamma_0 = \varepsilon\eta$ and $\Upsilon = \frac{Q(4\ln 2 - 1)}{2(1 + 2\ln 2)}$. Eq.(40) becomes :

$$\Phi_{i,j} = \Gamma_0 sech\left[\Gamma_0\sqrt{\Upsilon\Big(\frac{(i - v_{gx}t)^2}{A} + \frac{(j - 2v_{gy}t)^2}{B}\Big)}\right] \exp\left[i\Big(k_x a i + k_y j b - \Omega t\Big)\right] \tag{41}$$

with ω obtained in (23) then, we have:

$$\Omega = \omega - \frac{1}{12}\Big(4 - \frac{1}{\ln 2}\Big)Q\Gamma_0^2 = \mu - 2\Big[t_x \cos(k_x a) + t_y \cos(k_y b) + t_x^{'} \cos(2k_x a) + t_y^{'} \cos(2k_y b)\Big] + \frac{1}{12}\Big(4 - \frac{1}{\ln 2}\Big)B\Gamma_0^2 \tag{42}$$

To confirm the analytical studies, we present the numerical simulations of time evolution of the coherent amplitude $\phi(i,j)$ for certain couple of values of the wave number (k_x,k_y) obtained by solving the discrete NLS Eq.(5). The initial wave form considered is given in Eq. (41) with initial amplitude Γ_0 = 0.5 in the whole lattice at various time stages. where the size of the lattice is 400400. In the absence second neighbor hopping and for (k_x = π/55,k_y = π/55000), Figure.12 (a1)-(a3),(b1)-(b3) and (c1)-(c3) illustrates the time evolution of the coherent amplitude Φ(i,j) as follows: 1- at the initial time t = 0 ; 2- at time t = 50, and 3- at the final time t = 100. As we can see, the left column is the 3D plot, the middle is the modulus whereas the right denotes the projection in i = j plane. Figure.12 (a1)-(a3) clarifies how the breather changes its shape after it has completed t = 50, and t = 100 of oscillation respectively. During the propagation of the coherent amplitude $\phi(i,j)$, it is shown in panels (c1)-(c3) that, the amplitude changes its shape by exhibiting maximums and minimums over time. To evaluate the maximum breather amplitude, the modulus is plotted on panels (b1)-(b3), which confirms that the radial breather initially situated in the center of the lattice maintains its shape and amplitude at various time stages. Similar results were obtained by Yi and his co-worker working on stationary breather model in a 2D hexagonal spring-mass lattice [54].

However, in the presence of second neighbor hopping for the coupling strength t'_x = 0.9t_x, t'_y = 0.9ty and keeping the same value of the wavenumber as set in Figure.12, we realize on Figure.13 (a1)-(a3) that, the breather initially localized at the center of the lattice as shown on Figure.12 (a1)-(a3), has changed its shape by covering a large area than before by exhibiting more oscillation at various time stages. This oscillating behavior of the breather amplitude is clearly shown on Figure.13 (a1)-(a3) as the time increases. However panels (b1)-(b3) shown that, the inclusion of second neighbor hopping in the lattice, although the radial breather initially localized at the center of the lattice, maintains its amplitude and rests highly localized at various time stages, contribute significantly to spread its shape which covers a large area in the (i,j) plane as presented in panels (c1)-(c2). These results are in full agreement with the analytical studies.

From the numerical investigation, we can note that although the radial breather the maximum amplitude is more concentrated at center of the lattice in the absence of second neighbor hopping, the inclusion of second neighbor hopping continues to more spread the radial breather from the central, its maximum amplitude is still rested in the center of the lattice as time evolves meaning that the energy of the system is concentrated and the center of the lattice.

Conclusion and Discussion

We investigated the second-neighbor hopping effects on the MI and on the dynamics of breathers in 2D quantum ultracold atoms loaded in optical lattices. By using Glauber's coherent state method for bosonic operators, the equation of motion is obtained. The MI is studied by employing linear stability analysis. From the linear stability analysis, it is found that, the dispersion relation formed exhibits intriguing form displaying minimums and dramatic maximum of angular frequency at certain wavenumbers while the second neighbor hopping are included in this optical lattice. This result demonstrates that, the introduction of second neighbor hopping may affect the dispersion relation of the optical lattice. We also found the existence conditions of appearance of MI in the system. Our MI results revel, that the on-site interaction parameter have an important impact on the growth rate of the modulation waves amplitude, and on the appearance of the instability zones at the center and at the edges of the Brillouin zone depending on the sign of the on-site interaction parameter. The second neighbor hopping are also responsible to produce a change on the shape of the MI regions. The number of MI regions increases with the increasing second neighbor hopping coupling strength. Consequently, we can conclude that, the emergence of MI regions can be controlled by the second neighbor hopping coupling strength. Moreover, It also shown that the instability growth rate may be significantly affected by the second neighbor hopping coupling strength for certain values of the wavenumber. To support the analysis studies, direct numerical simulations of MI have been carried out to show that the generation of a train of short waves exhibiting periodic W-shaped and V-shaped solitons in the system with decreasing amplitude as time increases. These behaviors confirm the that, the plane wave is sensitive to any value of the wavenumber, the couple of points chosen which lies the instability region as example to propagate the modulated wave, manifests the modulation instability of the system and then validate the linear stability analysis prediction. Furthermore, by considering the fact that, the appearance of MI areas of plane waves is intimately linked to existence of breathers, we have predicted the emergence of breathers in the regions where the MI manifests and that this breather solution will be affected by the second neighbor hopping coupling strength. To reach the aim, by means of semi-discrete approximation associated with multiple-scale method, the NLSE is found. This equation is solved by making use of Rayleigh-Ritz variational method to study analytically and numerically the dynamics of breathers in the system. In agreement with the MI analysis, the analytical results have revealed the existence the radial symmetric modes called the dynamics of breathers. The accuracy of the analytical analysis outcomes was numerically checked by numerical calculations, where we have noticed that the inclusion of second neighbor hopping in the lattice, although the radial breather initially situated in the center of the lattice maintains its amplitude highly localized at various time stages, contribute significantly to spread its shape which covers a large area and validates the analytical predictions.

Our outcomes have been compared with those reported in reference [36], working in the same model with the absence of second neighbor hooping on which, the on-site interaction effects have been reported on the MI and the radial breathers whereas, in the present studies the second neighbor hooping are considered. More recently, similar results are been reported in reference where authors have applied asymptotic methods to find approximations to discrete breathers in a two dimensional hexagonal Fermi-Pasta-Ulam-KleinGordon lattice to find properties of breather in terms of stationary mode for two special wavenumbers $k = 0$ and $k = \pi$, with the difference that, in the present work, we have used Rayleigh-Ritz variational method in addition to linear stability analysis to investigate on the effects of second neighbor coupling on the MI and on the dynamics of breathers in 2D quantum ultracold atoms loaded in optical lattices [54]. Using semi-discrete limit in addition to low amplitude approximation, Pouget et al. examined the formation of localized structures which moved slowly, mediated by modulational instability, on a 2D lattice [55]. By using asymptotic methods and the multiple-scale some results suggested that long-lived stationary and moving breathers can be supported by the lattice [56,57]. Their stationary and moving breathers are similar to radial breather solution found in this work with the difference that, although the radial breather the maximum amplitude is more concentrated at center of the lattice in the absence of second neighbor hopping, the inclusion of second neighbor hopping continues to more spread the radial breather from the central, its maximum amplitude is still rested in the center of the lattice as time evolves meaning that the energy of the system is concentrated and the center of the lattice.

We point out here that, these unusual features effect of second neighbor hopping on the dynamics of breathers and on the MI have not yet been investigated before in the literature to our knowledge. We hoped that these results may enrich the knowledge on the dynamics of breathers can help to explain many phenomena observed in others nonlinear systems.

References

1. Anderson, M. H., Ensher, J. R., Matthews, M. R., Wieman, C. E., & Cornell, E. A. (1995). Observation of Bose-Einstein condensation in a dilute atomic vapor. science, 269(5221), 198-201.
2. DeMarco, B., & Jin, D. S. (1999). Onset of Fermi degeneracy in a trapped atomic gas. science, 285(5434), 1703-1706.
3. Davis, K. B., Mewes, M. O., Andrews, M. R., van Druten, N. J., Durfee, D. S., Kurn, D. M., & Ketterle, W. (1995). Bose-Einstein condensation in a gas of sodium atoms. Physical review letters, 75(22), 3969.
4. Jaksch, D., Bruder, C., Cirac, J. I., Gardiner, C. W., & Zoller, P. (1998). Cold bosonic atoms in optical lattices. Physical Review Letters, 81(15), 3108.
5. Bloch, I., Dalibard, J., & Zwerger, W. (2008). Many-body physics with ultracold gases. Reviews of modern physics, 80(3), 885-964.

6. Giuliano, D., Rossini, D., Sodano, P., & Trombettoni, A. (2013). XXZ spin-1 2 representation of a finite-U Bose-Hubbard chain at half-integer filling. Physical Review B Condensed Matter and Materials Physics, 87(3), 035104.
7. Greiner, M., Mandel, O., Esslinger, T., Hänsch, T. W., & Bloch, I. (2002). Quantum phase transition from a superfluid to a Mott insulator in a gas of ultracold atoms. nature, 415(6867), 39-44.
8. Fisher, M. P., Weichman, P. B., Grinstein, G., & Fisher, D. S. (1989). Boson localization and the superfluid-insulator transition. Physical Review B, 40(1), 546.
9. Bloch, I. (2005). Ultracold quantum gases in optical lattices. Nature physics, 1(1), 23-30.
10. Jaksch, D., Bruder, C., Cirac, J. I., Gardiner, C. W., & Zoller, P. (1998). Cold bosonic atoms in optical lattices. Physical Review Letters, 81(15), 3108.
11. Romanenko, V. I., Udovitskaya, Y. G., Romanenko, A. V., & Yatsenko, L. P. (2014). Cooling and trapping of atoms and molecules by counterpropagating pulse trains. Physical Review A, 90(5), 053421.
12. Prestipino, S. (2021). Bose-Hubbard model on polyhedral graphs. Physical Review A, 103(3), 033313.
13. Scott, A. C., & Eilbeck, J. C. (1994). H. Gilh j. Quantum lattice solitons. Physica D, 78, 194.
14. Flach, S., & Willis, C. R. (1998). Discrete breathers. Physics reports, 295(5), 181-264.
15. Flach, S., & Gorbach, A. V. (2008). Discrete breathers advances in theory and applications. Physics Reports, 467(1-3), 1-116.
16. MacKay, R. S., & Aubry, S. (1994). Proof of existence of breathers for time-reversible or Hamiltonian networks of weakly coupled oscillators. Nonlinearity, 7(6), 1623.
17. Tang, B. (2016). Quantum two-breathers formed by ultracold bosonic atoms in optical lattices. International Journal of Theoretical Physics, 55(6), 2697-2710.
18. Djoufack, Z. I., Kenfack-Jiotsa, A., & Nguenang, J. P. (2017). Quantum signature of breathers in 1D ultracold bosons in optical lattices involving next-nearest neighbor interactions. International Journal of Modern Physics B, 31(20), 1750140.
19. Djoufack, Z. I., Tala-Tebue, E., Fotsa-Ngaffo, F., Tsajio, A. D., & Kapche-Tagne, F. (2018). Quantum breathers associated with modulational instability in 1D ultracold boson in optical lattices involving next-nearest neighbor interactions. Optik, 164, 575-589.
20. Djoufack, Z. I., Tala-Tebue, E., & Nguenang, J. P. (2019). Quantum breathers and intrinsic localized excitation associated with the modulational instability in 1D Bose–Hubbard chain. Communications in Nonlinear Science and Numerical Simulation, 69, 134-147.
21. Kivshar, Y. S., & Peyrard, M. (1992). Modulational instabilities in discrete lattices. Physical Review A, 46(6), 3198.
22. Kivshar, Y. S. (1993). Localized modes in a chain with nonlinear on-site potential. Physics Letters A, 173(2), 172-178.
23. Lai, R., & Sievers, A. J. (1998). Modulational instability of nonlinear spin waves in easy-axis antiferromagnetic chains. Physical Review B, 57(6), 3433.
24. Stockhofe, J., & Schmelcher, P. (2016). Modulational instability and localized breather modes in the discrete nonlinear Schrödinger equation with helicoidal hopping. Physica D: Nonlinear Phenomena, 328, 9-20.
25. Baronio, F., Chen, S., Grelu, P., Wabnitz, S., & Conforti, M. (2015). Baseband modulation instability as the origin of rogue waves. Physical Review A, 91(3), 033804.
26. Gori, G., Macrì, T., & Trombettoni, A. (2013). Modulational instabilities in lattices with power-law hoppings and interactions. Physical Review E Statistical, Nonlinear, and Soft Matter Physics, 87(3), 032905.
27. Wang, L., Zhang, J. H., Wang, Z. Q., Liu, C., Li, M., Qi, F. H., & Guo, R. (2016). Breather-to-soliton transitions, nonlinear wave interactions, and modulational instability in a higher-order generalized nonlinear Schrödinger equation. Physical Review E, 93(1), 012214.
28. Benjamin, T. B., & Feir, J. E. (1967). The disintegration of wave trains on deep water Part 1. Theory. Journal of Fluid Mechanics, 27(3), 417-430.
29. Guo, D., Tian, S. F., Zhang, T. T., & Li, J. (2018). Modulation instability analysis and soliton solutions of an integrable coupled nonlinear Schrödinger system. Nonlinear Dynamics, 94(4), 2749-2761.
30. Hao, H. Q., Guo, R., & Zhang, J. W. (2017). Modulation instability, conservation laws and soliton solutions for an inhomogeneous discrete nonlinear Schrödinger equation. Nonlinear Dynamics, 88(3), 1615-1622.
31. Halboth, C. J., & Metzner, W. (2000). Renormalization-group analysis of the two-dimensional Hubbard model. Physical Review B, 61(11), 7364.
32. Beenen, J., & Edwards, D. M. (1995). Superconductivity in the two-dimensional Hubbard model. Physical Review B, 52(18), 13636.
33. Stanescu, T. D., Galitski, V., & Das Sarma, S. (2010). Topological states in two-dimensional optical lattices. Physical Review A Atomic, Molecular, and Optical Physics, 82(1), 013608.
34. Alba, V., Haque, M., & Läuchli, A. M. (2013). Entanglement spectrum of the two-dimensional bose-hubbard model. Physical review letters, 110(26), 260403.
35. Schönmeier-Kromer, J., & Pollet, L. (2014). Ground-state phase diagram of the two-dimensional Bose-Hubbard model with anisotropic hopping. Physical Review A, 89(2), 023605.
36. Djoufack, Z. I., Fotsa-Ngaffo, F., Tala-Tebue, E., Fendzi-Donfack, E., & Kapche-Tagne, F. (2019). Modulational instability in addition to discrete breathers in 2D quantum ultracold atoms loaded in optical lattices. Nonlinear Dynamics, 98(3), 1905-1918.
37. Gao, Y. E., & Han, F. (2008). Effects of the next-nearest-neighbor hopping in optical lattices. Modern Physics Letters B, 22(01), 33-44.
38. Kibey, A., Sonone, R., Dey, B., & Eilbeck, J. C. (2015). Quantization of β-Fermi–Pasta–Ulam lattice with nearest and

next-nearest neighbor interactions. Physica D: Nonlinear Phenomena, 294, 43-53.
39. Lin, H. Q., & Hirsch, J. E. (1987). Two-dimensional Hubbard model with nearest-and next-nearest-neighbor hopping. Physical Review B, 35(7), 3359.
40. Fontenele, R. A., Vasconcelos, N., Costa, N. C., Paiva, T., & dos Santos, R. R. (2023). Second-neighbor hopping effects in the two-dimensional attractive Hubbard model. Condensed Matter, 8(1), 11.
41. Djoufack, Z. I., Tala-Tebue, E., Nguenang, J. P., & Kenfack-Jiotsa, A. (2016). Quantum soliton in 1D Heisenberg spin chains with Dzyaloshinsky-Moriya and next-nearest-neighbor interactions. Chaos: An Interdisciplinary Journal of Nonlinear Science, 26(10).
42. Tang, B. (2016). Quantum Breathers in Anisotropy Ferromagnetic Chains with Second-Order Coupling. International Journal of Theoretical Physics, 55(8), 3657-3671.
43. Tala-Tebue, E., Djoufack, Z. I., Kenfack-Jiotsa, A., Kapche-Tagne, F., & Kofané, T. C. (2017). Second neighbors inducing common frequencies for bright and dark solitons. The European Physical Journal Plus, 132(6), 272.
44. Reich, S., Maultzsch, J., Thomsen, C., & Ordejon, P. (2002). Tight-binding description of graphene. Physical Review B, 66(3), 035412.
45. Deacon, R. S., Chuang, K. C., Nicholas, R. J., Novoselov, K. S., & Geim, A. K. (2007). Cyclotron resonance study of the electron and hole velocity in graphene monolayers. Physical Review B Condensed Matter and Materials Physics, 76(8), 081406.
46. Glauber, R. J. (1963). Coherent and incoherent states of the radiation field. Physical Review, 131(6), 2766.
47. Smith, H. (1991). Introduction to quantum mechanics. World scientific.
48. Abdullaev, F. K., Bouketir, A., Messikh, A., & Umarov, B. A. (2007). Modulational instability and discrete breathers in the discrete cubic–quintic nonlinear Schrödinger equation. Physica D: Nonlinear Phenomena, 232(1), 54-61.
49. Daumont, I., Dauxois, T., & Peyrard, M. (1997). Modulational instability: first step towards energy localization in nonlinear lattices. Nonlinearity, 10(3), 617.
50. Djoufack, Z. I., Tala-Tebue, E., Nguenang, J. P., & Kenfack-Jiotsa, A. (2021). Radial solitons and modulational instability in two-dimensional Ablowitz-Ladik equation for certain applications in nonlinear optics. Optik, 225, 165639.
51. Remoissenet, M. (1986). Low-amplitude breather and envelope solitons in quasi-one-dimensional physical models. Physical Review B, 33(4), 2386.
52. Remoissenet, M.: Waves Called Solitons, Concepts and Experiments. third ed. SpringerVerlag, Berlin (1999)
53. Butt, I. A., & Wattis, J. A. (2006). Discrete breathers in a two-dimensional Fermi–Pasta–Ulam lattice. Journal of Physics A: Mathematical and General, 39(18), 4955.
54. Yi, X., & Liu, S. (2020). Stationary breather model in a two-dimensional hexagonal spring-mass lattice. Nuclear Physics B, 951, 114884.
55. Pouget, J., Remoissenet, M., & Tamga, J. M. (1993). Energy self-localization and gap local pulses in a two-dimensional nonlinear lattice. Physical Review B, 47(22), 14866.
56. Butt, I. A., & Wattis, J. A. (2007). Discrete breathers in a two-dimensional hexagonal Fermi–Pasta–Ulam lattice. Journal of Physics A: Mathematical and Theoretical, 40(6), 1239.
57. Wattis, J. A., & James, L. M. (2014). Discrete breathers in honeycomb Fermi–Pasta–Ulam lattices. Journal of Physics A: Mathematical and Theoretical, 47(34), 345101.